Available online at www.sciencedirect.com
ScienceDirect
Journal of Catalysis 255 (2008) 29–39
JOURNAL OF CATALYSIS
www.elsevier.com/locate/jcat

Mechanism of HCl oxidation (Deacon process) over RuO_2

Núria López [a,*], Jordi Gómez-Segura [a], Raimon P. Marín [a], Javier Pérez-Ramírez [a,b,*]

[a] *Institute of Chemical Research of Catalonia (ICIQ), Avinguda Països Catalans 16, 43007 Tarragona, Spain*
[b] *Catalan Institution for Research and Advanced Studies (ICREA), Passeig Lluís Companys 23, 08010 Barcelona, Spain*

Received 20 August 2007; revised 16 January 2008; accepted 21 January 2008

Abstract

The catalytic oxidation of hydrogen chloride to chlorine (Deacon reaction) is an attractive means to recover Cl_2 from HCl-containing waste streams in the chemical industry. Recently, RuO_2 supported on TiO_2 rutile has been industrially implemented for large-scale chlorine manufacture. However, detailed understanding of the reaction mechanism over claimed catalysts has not been acquired. Our tests in a fixed-bed reactor at ambient pressure concluded that RuO_2 powder is highly active for Cl_2 production. Characterization of the fresh and used RuO_2 samples by *ex situ* XRD and XPS revealed no appreciable alteration of the bulk structure and limited chlorination of the catalyst. *Ab initio* thermodynamics predicted that the initial state of the $RuO_2(110)$ surface is partially over-oxidized, while the surface after reaction contains both oxygen and chlorine. DFT described the Deacon reaction with a Mars–van Krevelen type mechanism consisting of five steps: hydrogen abstraction from HCl, recombination of atomic chlorine, hydroxyl recombination, water desorption, and dissociative oxygen adsorption. An increased chlorine production was observed experimentally when increasing the feed O_2-to-HCl ratio. This can be ascribed both to the lower recombination energy of chlorine atoms to gas-phase Cl_2 at high coverages and the faster surface reoxidation due to higher partial oxygen pressures.

Keywords: HCl oxidation; Chlorine; Deacon reaction; RuO_2; Mechanism; Density Functional Theory; On-line Cl_2 analysis; *Ab initio* thermodynamics

1. Introduction

Elemental chlorine (Cl_2) is widely used in the production of a wide range of industrial and consumer products. Approximately 50% of the chlorine produced worldwide (ca. 50 Mton per annum) is reduced through its use to HCl or chloride salts [1]. An example of particular relevance is the phosgenation of diamines to diisocyanates (Eq. (1)) as the first step to manufacture polyurethane resins and rubbers. This reaction leads to 4 mole of HCl per mole of diisocyanate.

$$R(NH_2)_2 + COCl_2 \rightarrow R(NCO)_2 + 4HCl. \quad (1)$$

The by-product HCl can be generally marketed as hydrochloric acid or used as a raw material in vinyl chloride monomer (VCM) production. However, as the VCM production growth is slow, excess supply of HCl is foreseen. In these cases, this highly toxic and corrosive acid must be neutralized. Besides, the main Cl_2 production method, salt electrolysis, is energy intensive and encompasses the disadvantage of producing caustic soda. Thus, large-scale manufacturers aim at the development of a chlorine recycling technology due to environmental and economic reasons.

An attractive route for chlorine recovery is the gas-phase catalytic oxidation of HCl with air or oxygen (Eq. (2)), the so-called Deacon reaction [2–4], due to the relative ease of application and low electrical power and thermal requirements when compared with electrolytic processes. The reaction is reversible and exothermic ($\Delta H^0 = -28.4$ kJ mol^{-1} HCl):

$$4HCl + O_2 \leftrightarrow 2Cl_2 + 2H_2O. \quad (2)$$

From the various systems protected by Henry Deacon in the late 19th century, $CuCl_2$ supported on pumice was the preferred one. However, catalytic tests in a fixed-bed reactor at 703–773 K evidenced serious drawbacks for implementation: low single-pass HCl conversion due to limited activity, rapid deactivation due to volatilization of copper chloride above 673 K, and corrosion problems due to the presence of unreacted HCl and product H_2O [4]. Many efforts have been undertaken since

* Corresponding authors. Fax: +34 977 920 224.
E-mail addresses: nlopez@iciq.es (N. López), jperez@iciq.es (J. Pérez-Ramírez).

0021-9517/$ – see front matter
doi:10.1016/j.jcat.2008.01.020

then for developing more efficient systems, culminating with the Shell-Chlor process (Shell) in the 1960s and the MT-Chlor process (Mitsui Toatsu Chemicals) in the late 1980s. The Shell-Chlor process made use of a single fluidized-bed reactor with a $CuCl_2$–KCl/SiO_2 catalyst [5,6], but it was abandoned due to limited HCl conversion and severe corrosion problems. The MT-Chlor process utilizes a Cr_2O_3/SiO_2 catalyst in a fluidized-bed reactor at 623–673 K [7–9]. Presently, Mitsui Toatsu is operating a 50 kton per annum plant based on the MT-Chlor process at Omuta, Japan. In the late 1990s, Totsis et al. [10,11] developed a dual fluidized-bed reactor system using copper-based catalysts in order to achieve high HCl conversion to Cl_2 with minimal corrosion. In the same line as Totsis et al., Nieken and Watzenberger [12] demonstrated that periodic operation of the Deacon process in a two-step fixed-bed reactor can overcome corrosion problems.

A wider scope for industrialization of the one-step hydrochloric acid oxidation process has been realized through the development by Sumitomo Chemicals of a process using a RuO_2 supported on TiO_2 rutile catalyst in a fixed-bed reactor configuration [13]. Not surprisingly, RuO_2–TiO_2 coated titanium anodes are industrially used for chlorine evolution in NaCl electrolytic cells [14,15]. The RuO_2/TiO_2 catalyst exhibits high activity at low temperature and remarkable stability, leading to Cl_2 with higher purity than that obtained by NaCl electrolysis. Besides, the chlorine manufacturing cost is claimed to be much lower than that of electrolysis and the MT-Chlor process due to the low electric power consumption and efficient heat recovery from the reaction. The Sumitomo process can produce up to 400 kton of chlorine per annum in a single reactor [16].

The vast number of patents claiming Deacon-type catalysts and reactors contrasts with the scarce number of fundamental studies dealing with mechanistic and kinetic aspects of the reaction. Hisham and Benson [17] studied the basic thermochemistry of the Deacon reaction over a number of metal oxides. The process was examined in two steps: (1) HCl absorption by the metal oxide to form the metal (oxy)chloride and (2) the oxidation of the latter by O_2 to regenerate the metal oxide and free Cl_2. CuO was concluded as the only system fulfilling the requirements of a complete cycle below 700 K, although RuO_2 was not included in the study. Exceptionally, Aglulin [18] investigated the kinetics of HCl oxidation over supported Cr_2O_3 catalysts in the presence of methane, although some of the steps in the hypothesized mechanism cannot be considered as elementary.

Consequently, deeper mechanistic studies of the Deacon reaction over ruthenium oxide are required in order to better understand how the industrial catalyst works. This information can also be beneficial for further catalyst optimization. RuO_2 has received considerable attention over the past years as model system for surface science and computational studies, and also as heterogeneous catalyst in oxidation of various substrates, among others carbon monoxide [19–23], hydrogen [24–26], ammonia [27], methane [28], alcohols [21,29–31], and soot [32].

Herein we have used experiments and Density Functional Theory (DFT) to study the mechanism of HCl oxidation to Cl_2 over RuO_2 surfaces. Previous to the simulations, evidence that polycrystalline RuO_2 powder is active in the Deacon reaction has been obtained at different feed $HCl:O_2$ ratios by means of catalytic tests in a continuous fixed-bed reactor at ambient pressure. A reaction mechanism comprising five fundamental steps has been identified and characterized. In particular, the effect of surface coverage and the nature of the active oxygen species on RuO_2 have been analyzed. The fresh and used RuO_2 samples have been characterized in order to assess eventual changes in the bulk and surface of the catalyst upon reaction.

2. Experimental

2.1. Catalyst characterization

Ruthenium(IV) oxide, RuO_2, was purchased from Sigma-Aldrich. Prior to characterization and catalytic tests, the as-received sample was heated in static air from 298 to 773 K at 5 K min^{-1} and kept isothermal for 5 h. Powder X-ray diffraction (XRD) was measured in transmission using a Bruker AXS D8 Advance diffractometer equipped with a Cu tube, a Ge(111) incident beam monochromator ($\lambda = 0.1541$ nm), and a Vantec-1 PSD. Data were recorded in the 2θ range of 5 to 70° with an angular step size of 0.016° and a counting time of 2.4 s per step. X-ray photoelectron spectroscopy (XPS) analyses were obtained using a PHI 5500 Multitechnique System from Physical Electronics equipped with an ultrahigh vacuum chamber (pressure between 5×10^{-9} and 2×10^{-8} Torr) and monochromatic Al$K\alpha$ radiation at 1486.6 eV as the X-ray source. Nitrogen adsorption–desorption isotherms at 77 K were measured on a Quantachrome Autosorb 1MP analyzer. Before analysis, the sample was degassed in vacuum at 393 K for 12 h. The BET method [33] was applied to determine the total surface area.

2.2. Activity tests

The catalytic oxidation of HCl over RuO_2 was studied in a quartz fixed-bed reactor (8 mm i.d.) using 600 mg of sample (sieve fraction 200–300 μm), a total pressure of 1 bar, and a weight-hourly space velocity (WHSV) was 16,600 ml g^{-1} h^{-1}. The feed mixture contained 20 vol% HCl, 20–80 vol% O_2, and N_2 as the balance gas. Hydrogen chloride (Praxair, purity 3.0 and water content <50 ppm), oxygen (Carburos Metálicos, purity 3.5), and nitrogen (Carburos Metálicos, purity 3.5) were used without further purification. The individual gases were introduced to the reactor by means of digital mass-flow controllers. The material of all the lines in the set-up was Teflon® in order to prevent corrosion problems, particularly downstream of the reactor. Two protocols were applied for catalytic evaluation. Temperature-programmed reaction (TPR) was carried out by ramping the temperature of the reactor block (T_{furnace}) from 333 to 583 K at 10 K min^{-1} in the reaction mixture. The catalyst was pretreated in a 40 vol% O_2 in N_2 at 333 K for 20 min prior to HCl admission. Isothermal tests were conducted

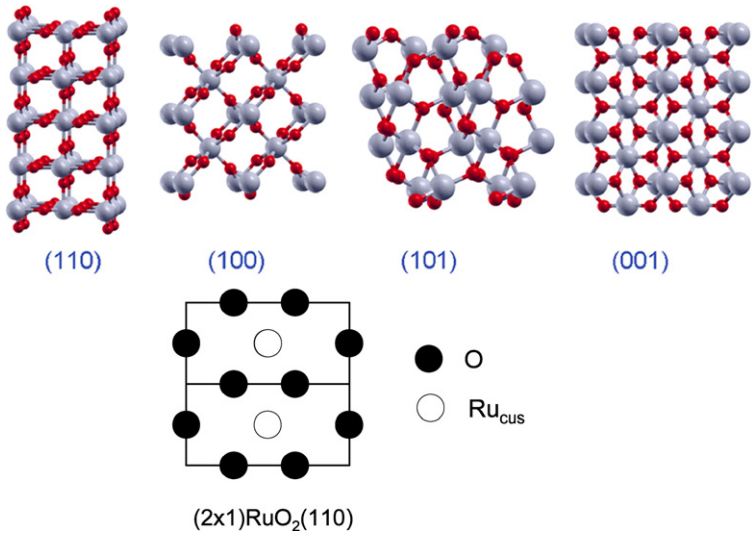

Fig. 1. Ball and stick model of different RuO_2 surfaces. In the upper panel, oxygen and ruthenium atoms are represented by red and grey spheres, respectively. In the lower panel the notation for the $RuO_2(110)$ surface is presented in a $p(2 \times 1)$ supercell. (For interpretation of the references to color in this figure legend, the reader is referred to the web version of this article.)

at $T_{furnace} = 573$ K using molar HCl:O_2 ratios in the feed of 1:1, 1:2, 1:3, and 1:4. The temperature was ramped from 333 to 573 K at 10 K min^{-1} in 20 vol% O_2 in N_2 and HCl was subsequently introduced in the feed. The HCl:O_2 ratio was varied by increasing the inlet O_2 concentration and the inlet HCl concentration was fixed at 20 vol%. The flow of N_2 was adjusted in order to keep a constant total flow (10 l STP h^{-1}). During the tests, the catalyst bed temperature was continuously recorded with a Fluke Digital Multimeter (model 187) equipped with a K-type thermocouple.

Chlorine analysis was carried out using an Ocean Optics miniature fiber optic spectrophotometer (model USB2000-UV-VIS). Spectra were collected in the broad wavelength range of 200–1000 nm every 10 s using a DT-MINI-2-GS Deuterium Tungsten Halogen Light Source and a high-sensitivity Sony ILX511 2048-element linear silicon CCD-array detector upgraded for working in the UV spectral region. On-line Cl_2 detection via optical absorbance measurements was achieved by the continuous flow of product gases through a Z-flow cell adopted as flow injection analysis (FIA) type assembly having a 10-mm optical path length (FIAlab instruments). Water produced in the reaction was condensed using a reflux unit prior to the detection cell. The carrier gas (N_2) provided a reference spectrum in optical absorbance processing.

3. Computational details

Density Functional Theory (DFT) was applied to study the mechanism of HCl oxidation to Cl_2 on RuO_2. Calculations have been performed with the VASP code [34,35], employing the RPBE functional [36], the inner electrons have been represented by PAW pseudopotentials [37], and the valence monoelectronic states have been expanded in plane-waves with a cutoff energy of 400 eV. RuO_2 has a rutile structure [38] and is consequently isostructural to the most stable TiO_2 polymorph. The unit cell parameters obtained with our set up ($a = b = 4.569$ Å, $c = 3.140$ Å and $u = 0.305$) are in good agreement with the experimentally determined values using single-crystal X-ray diffraction [39]. The good accuracy of a similar approach when compared to all electron calculations was tested in Ref. [40].

In a first step, the low-index (110), (101), (001), and (100) surfaces were modeled (Fig. 1). The slabs contained at least 5 layers of RuO_2 and the vacuum space between the different slabs was set to >10 Å, with a k-point sampling density of at least 0.4 Å^{-1}. The outermost 2 layers in the slabs were allowed to relax. The surface energies, calculated for the stoichiometric termination of each of the facets, were in agreement with previous estimates [41], leading to (110) as the most stable surface with $\gamma = 0.90$ J m^{-2}.

The clean $RuO_2(110)$ structure consists on alternating rows of protruding oxygen atoms, usually denoted as O_b (bridge oxygen) and rows of coordinatively unsaturated ruthenium atoms, Ru_{cus}, along the [001] direction. For mechanistic studies, the (110) surface of RuO_2 has been represented by a 3-layer slab separated by 15.7 Å, where each of the layers contains an $ORuO_2O$ sub-unit. Relaxation was only allowed in the two first layers of the slab keeping the lower layer fixed. In order to avoid spurious electrostatic interactions, the dipole arising from the formation of an asymmetric surface was eliminated from the vacuum. To study adsorption and reaction processes the supercell employed was a $p(2 \times 1)$ reconstruction, leading to a coverage by H, Cl, or O_{cus} of 0.50 ML. Tests with a larger supercell $p(4 \times 1)$ were performed to study the atomic chlorine recombination to gas-phase Cl_2 and the O_2 adsorption. A Monkhorst–Pack [42] mesh was employed to perform the numerical integration; the meshes contain $4 \times 4 \times 1$ points for the small supercell and reduced to $2 \times 4 \times 1$ for the larger cell. The barriers of relevant elementary steps have been calculated using the CI-NEB [43].

RuO_2 is a partially covalent oxide and thus formal charges on Ru and O differ from the real charges of the atoms. RuO_2 is thus reducible via O_2 elimination but also the surface can be

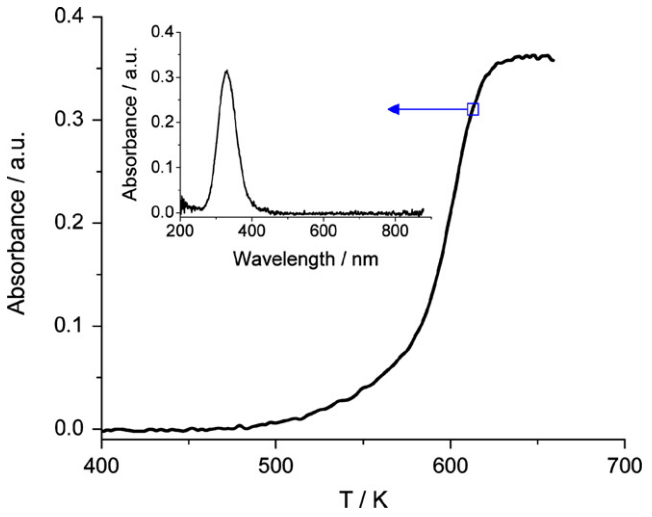

Fig. 2. Absorbance due to Cl_2 production during temperature-programmed reaction of HCl with O_2 over RuO_2. Conditions: feed mixture of 20 vol% HCl and 40 vol% O_2 in N_2, GHSV = 16,600 h^{-1}, $P = 1$ bar. Inset: UV–vis spectrum at a particular temperature, showing the Cl_2 band centered at 330 nm.

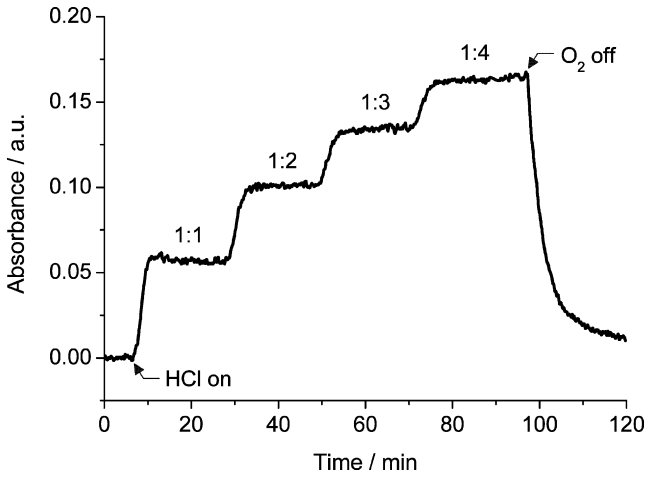

Fig. 3. Absorbance due to Cl_2 production in isothermal tests over RuO_2 at different molar HCl:O_2 ratios. Conditions: feed mixture of 20 vol% HCl and 20–80 vol% O_2 in N_2, $T_{furnace} = 573$ K, GHSV = 16,600 h^{-1}, $P = 1$ bar.

further oxidized in the Ru_{cus} centers. Under relevant pressures, the surface Ru_{cus} centers on $RuO_2(110)$ can be partially covered [44]. We have employed *ab initio* thermodynamics [45,46] to obtain the most likely composition of the $RuO_2(110)$ surface at 573 K in the presence of O_2 and Cl_2. The thermodynamic parameters for gas-phase oxygen or chlorine were taken from the NIST reference tables [47]. In the initial state, only O_2 is in contact with the surface, thus several O_b and O_{cus} coverages were calculated in a $p(4 \times 1)$ supercell and represented as a function of the oxygen pressure. To represent the state of the surface after reaction, a $p(2 \times 1)$ supercell was employed where both O_b and Ru_{cus} positions can be occupied by either O or Cl. In fact, O_b substitution by Cl is energetically possible, the reaction being exothermic by −0.15 eV. Moreover, the Cl_b containing structure constitutes an energy minimum that can be characterized by the lack of imaginary vibrational frequencies. The electronic structure of Ru–Cl_b–Ru can be seen as a three center-three electron bond with partially oxidized Ru atoms although with a different atomic charge than that of the clean RuO_2. This is possible due to the redox character of Ru that can accept formal charges of +2, +3, and +4. In contrast, double Cl substitution (i.e. 2Cl in the position of O_b) is an endothermic process (by 2 eV) and thus not likely. This is similar to what has been shown for the phase diagram of RuO_2 in the presence of CO and O, where CO and O can occupy both bridge and cus positions [44]. The large number of configurations arising (21 for the $p(2 \times 1)$ supercell) when compared to the case of oxygen (5 for $p(4 \times 1)$) prevented us from using a more realistic supercell.

4. Results and discussion

4.1. Deacon performance of RuO_2 powder

Fig. 2 shows the absorbance profile due to Cl_2 production *vs* the temperature of the catalyst bed during a temperature-programmed reaction experiment over RuO_2 powder at a molar feed HCl:O_2 ratio of 1:2 and atmospheric pressure. The onset temperature is around 500 K and the absorbance progressively increases until reaching a plateau around 625 K with a value of absorbance of 0.35. Acquisition data for absorption spectrum using the combined-spectrum source ranging between 200–410 nm (deuterium lamp) and 360–1000 nm (tungsten halogen lamp) is unambiguously indicative of the selective detection of pure chlorine in the UV spectral region, exhibiting the maximum absorbance at 330 nm (inset in Fig. 2) [48–50]. The saturation of the detector was determined at 1.1 units of absorbance, below which a linear relationship between the absorbance and the Cl_2 concentration was observed.

The influence of the HCl:O_2 ratio on the Deacon activity of RuO_2 was investigated at $T_{furnace} = 573$ K. As shown in Fig. 3, the absorbance increases upon increasing the relative amount of oxygen in the feed mixture. Interruption of O_2 causes a rapid drop of absorbance due to the diminished Cl_2 production. The beneficial effect of oxygen on the Cl_2 production is further discussed in Section 4.3 attending to simulation results at different oxygen coverages. The single-pass HCl conversion in the isothermal experiment at HCl:O_2 = 1:2 was quantified at ca. 70% by classical titration. To this end, the Cl_2 concentration of the outlet gas was determined after passing through two serial impingers over 10 min, each of which equipped with a porous frit immersed into an aqueous solution of potassium iodide (20–30 wt%). The iodine thus obtained was titrated with sodium thiosulfate (0.1 M).

Consequently, the high activity of RuO_2-based catalysts in the Deacon process claimed by Sumitomo [13] can be confirmed on the basis of the low onset temperature measured in temperature-programmed reaction experiments and the relatively high HCl conversion determined in steady-state tests over unsupported ruthenium oxide.

4.2. Characterization of fresh and used RuO_2

The XRD pattern of the fresh RuO_2 in Fig. 4 shows the characteristic reflections of ruthenium(IV) oxide (JCPDS 40-1290), with (110) and (101) as the prevailing primary orientations.

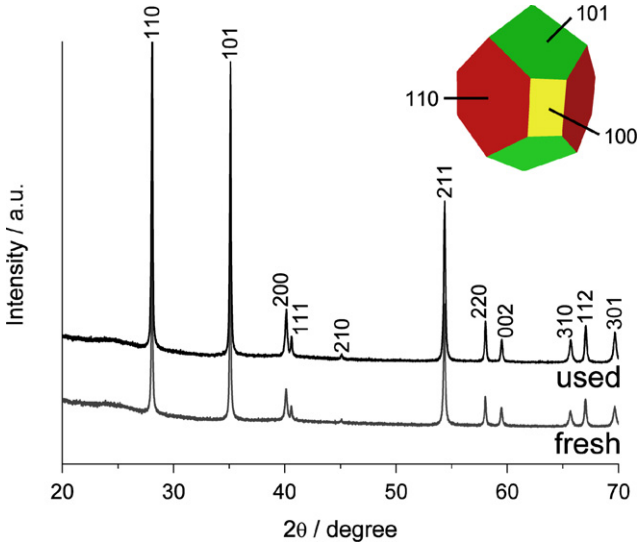

Fig. 4. X-ray diffraction patterns of the fresh and used RuO_2 samples. Inset: Wulff construction of the powder with the calculated surface energies for the facets in Fig. 1.

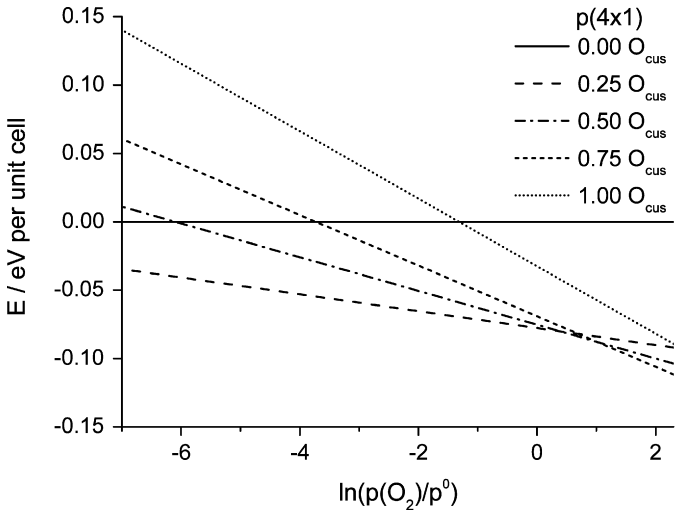

Fig. 5. *Ab initio* thermodynamics diagram of the surface composition of RuO_2(110) as a function of the O_2 pressure at 573 K.

We have performed calculations on the (110), (100), (101), and (001) facets of RuO_2 (see Fig. 1). The (110) facet is the lowest in energy and thus found in the largest extension when employing the Wulff construction [51] to build the structure of a nanoparticle (inset of Fig. 4). Moreover, in the TiO_2 rutile used as the support for RuO_2 in the Sumitomo catalyst [13,16], the (110) surface is the most stable too [52]. Accordingly, further DFT mechanistic studies concentrated on the RuO_2(110) surface. The choice of the (110) facet for calculations and the polycrystalline sample for catalytic tests can be justified. Temperature-programmed reaction studies over RuO_2(110) in UHV and polycrystalline RuO_2 at high-pressure conditions are virtually identical [21], indicating that the reaction pathways are very much alike and therefore the active centers on RuO_2 are the same. In addition, it is also known that the efficiency for CO oxidation hardly depends on the orientation of RuO_2 [53], at least not when the (110), (100), and (101) facets are compared, since all three low-energy surfaces contain five-fold coordinated ruthenium atoms, Ru_{cus} (see Fig. 1). In addition, the results from *ab initio* thermodynamics shown in Fig. 5 indicate that under the experimental conditions, a partial occupation of the Ru_{cus} atoms on the surface is likely. The state of the initial active surface in the presence of the gas-phase O_2 pressures contains all the O_b sites occupied and coverage of O_{cus} in the range of 0.25–0.75 ML.

The used RuO_2 sample resulting from temperature-programmed reaction experiments was characterized *ex situ* in order to assess changes due to the reaction. It should be recalled that the catalyst was subjected to a ramp of 5 K min^{-1} from 333 to 583 K in a mixture of 20 vol% HCl, 40 vol% O_2, and 40 vol% N_2 and the final temperature was kept for 1 h. Thereafter, the reactor was rapidly cooled down to room temperature in N_2 flow. The X-ray diffraction pattern of the used sample did not experience apparent changes with respect to the fresh one (Fig. 4). The position and relative intensity of the reflections of the RuO_2 phase were very similar and in particular no crystalline ruthenium oxychloride such as $RuOCl_2$ was observed after reaction. This indicates that the bulk of the catalyst was not altered by the Deacon test. The BET surface area of the fresh catalyst (10 $m^2\ g^{-1}$) decreased to 2 $m^2\ g^{-1}$ in the used one, suggesting some degree of sintering of the RuO_2 particles. X-ray photoelectron spectroscopy was conducted in order to investigate changes in the nature of the ruthenium species and to determine the extent of chlorination of the surface. The core level peaks of Ru 3d, O 1s, and Cl 2p are illustrated in Fig. 6 for the used RuO_2 catalyst, i.e. after Deacon reaction. The binding energy of ruthenium and oxygen (Ru $3d_{5/2}$ at 281 eV, Ru $3d_{3/2}$ at 285 eV, and O 1s at 529 eV) is characteristic of polycrystalline RuO_2 [21] and was identical in the fresh and used samples. This suggests that the Deacon reaction does not induce significant changes in the oxidation state of surface ruthenium sites in the tested period. The distinctive feature of the fresh and used RuO_2 specimens was the presence of chlorine in the latter sample, as shown in Fig. 6 by the Cl $2p_{3/2}$ (198 eV) and Cl $2p_{1/2}$ (199.5 eV) peaks. This demonstrates a certain degree of surface chlorination caused by HCl oxidation, although we cannot conclusively distinguish the nature of chlorine, i.e. whether it is as molecular chlorine solvated, hydrochloric acid solvated, or in the form of a surface oxychloride species. In any case, the minor amount of chlorine is limited to the catalyst surface. Accordingly, the use of an oxide, rather than a chlorinated compound, for DFT modelling is justified. In line with XPS analysis, application of other characterization methods such as far-infrared and Raman spectroscopies, temperature-programmed desorption coupled to mass spectrometry, and chemical analysis detected virtually no chlorine in the used RuO_2 catalyst. The practically unaltered state of RuO_2 after the Deacon reaction highlights the stability of this catalyst and likely explains its successful implementation as compared to other oxides based on copper and chromium, where extensive volatilization upon formation of the corresponding (oxy)chlorides has been observed. Future work will consider application of *operando* spectroscopic techniques to monitor the Deacon reaction. This approach proved successful to assess the chlorination at both surface and bulk levels of

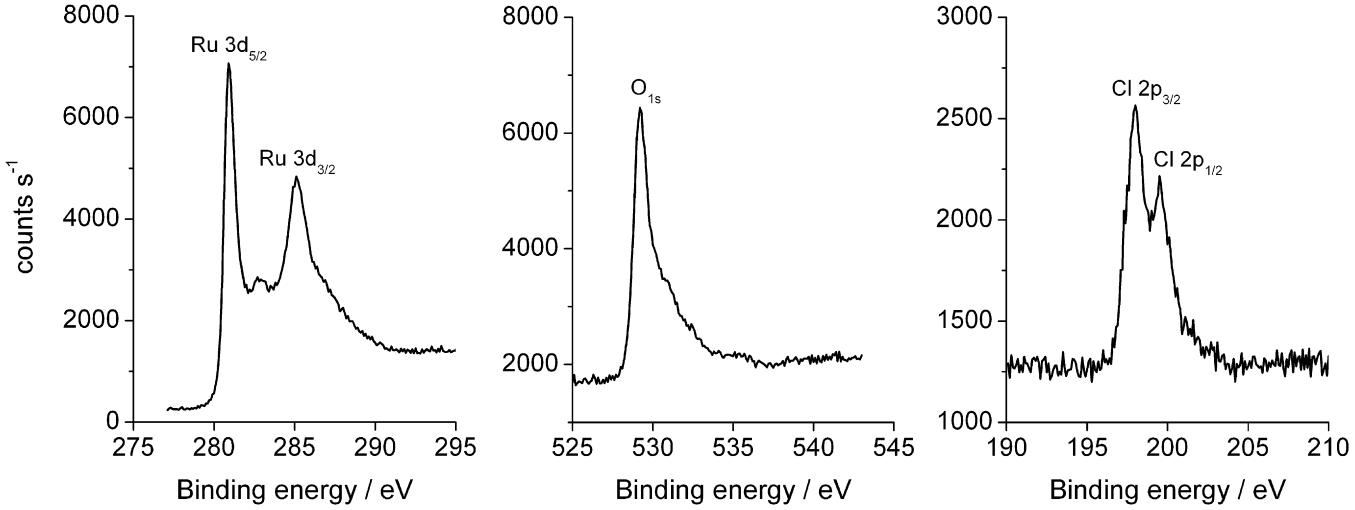

Fig. 6. XPS spectra of Ru 3d (left), O 1s (center) and Cl 2p (right) core level electrons of the RuO_2 catalyst used in the Deacon reaction.

lanthanide oxide-based catalysts during the destruction of CCl_4 in the presence of steam [54].

For the used catalyst, the $RuO_2(110)$ structure shall be in equilibrium with both Cl_2 and O_2. In this case the *ab initio* thermodynamics are much more complex, the configurations included in the search are reported in top Fig. 7 while the energy diagram is shown in bottom Fig. 7. The most likely configurations at relevant O_2 and Cl_2 pressures contain bridging sites occupied mostly with oxygen, the complete substitution of O_b atoms by Cl_b is energetically unfavored (by more than 1 eV with respect to the clean surface), thus suggesting that complete chlorination of the surface is indeed unlikely. The Ru_{cus} sites are also partially occupied, however, in this position Cl is more likely than O. Although partial substitution of O_b by Cl is energetically favored under equilibrium conditions, care must be taken since the elimination of O_b from the surface is highly endothermic (1.95 eV with respect to gas-phase O_2) and the kinetics of replacement can not compete with other less energy demanding processes like O_2 desorption from Ru_{cus} sites.

4.3. Reaction mechanism

The mechanism of the overall Deacon reaction (Eq. (2)) on $RuO_2(110)$ can be structured in five steps: hydrogen abstraction from hydrogen chloride by adsorbed atomic oxygen (Eq. (3)), recombination of surface chlorine atoms and desorption as gas-phase Cl_2 (Eq. (4)), recombination of surface hydroxyl groups (Eq. (5)), water desorption (Eq. (6)), and dissociative oxygen adsorption for surface regeneration (Eq. (7)). Although the above reaction scheme appears relatively simple, the complexity of the real process is large due to the distinct nature of the oxygen species on the surface and the different oxygen and chlorine coverage. Accordingly, each of the simplified steps in the reaction can occur in different scenarios. For instance, O* in Eqs. (3) and (5) can be either O_{cus} or O_b and each case has to be computed separately. In consequence, we have studied the reaction network at distinct degrees of surface oxidation and chlorination.

$$HCl + O^* + * \leftrightarrow OH^* + Cl^*, \tag{3}$$

$$Cl^* + Cl^* \leftrightarrow Cl_2 + 2^*, \tag{4}$$

$$OH^* + OH^* \leftrightarrow H_2O^* + O^*, \tag{5}$$

$$H_2O^* \leftrightarrow H_2O + *, \tag{6}$$

$$O_2 + 2^* \leftrightarrow 2O^*. \tag{7}$$

4.3.1. Hydrogen abstraction from hydrogen chloride

The first step in the mechanism is the hydrogen abstraction from HCl leading to adsorbed atomic chlorine and hydroxyl species (Eq. (3)). Three dissociation scenarios were investigated by using different oxygen coverages (Fig. 8). For the regular (110) surface, the bridge oxygen (O_b) can act as the basic center to dissociate hydrogen chloride. In the initial state, the HCl molecule is bonded through electrostatic interaction to O_b. This adsorbed state is determined −0.48 eV below the gas-phase reactants. For this structure, the relevant geometric parameters are $d(O_b–H) = 1.780$, $d(H–Cl) = 1.358$, and $d(Cl–Ru_{cus}) = 2.668$ Å. The H–Cl distance is already longer than that in the gas-phase molecule, i.e. $d(H–Cl) = 1.274$ Å. Dissociation of the HCl is exothermic by −0.98 eV and leads to a bridging hydroxyl group (O_bH) and a chlorine atom adsorbed on the Ru_{cus} position (denoted as Cl_{cus}). The geometric parameters in the final state are $d(O_b–H) = 0.992$, $d(H–Cl) = 2.278$, and $d(Cl–Ru_{cus}) = 2.361$ Å. At the transition state, $E_a = 0.05$ eV, the hydrogen atom is midway between the oxygen and the chlorine atoms, i.e. $d(O_b–H) = 1.702$, $d(H–Cl) = 1.371$, and $d(Cl–Ru_{cus}) = 2.672$ Å. The basic features of this elementary step are not affected by the presence of Cl_{cus} atoms in the Ru neighboring to the Ru_{cus} active site, top right Fig. 8. The HCl adsorption is reduced to −0.12 eV and dissociation is slightly less exothermic (−0.93 eV) compared to the clean surface, while the dissociation barrier is even smaller than 0.05 eV.

When a partially O-covered Ru_{cus} exists on the surface (see bottom Fig. 8), an alternative reaction path is feasible. In the

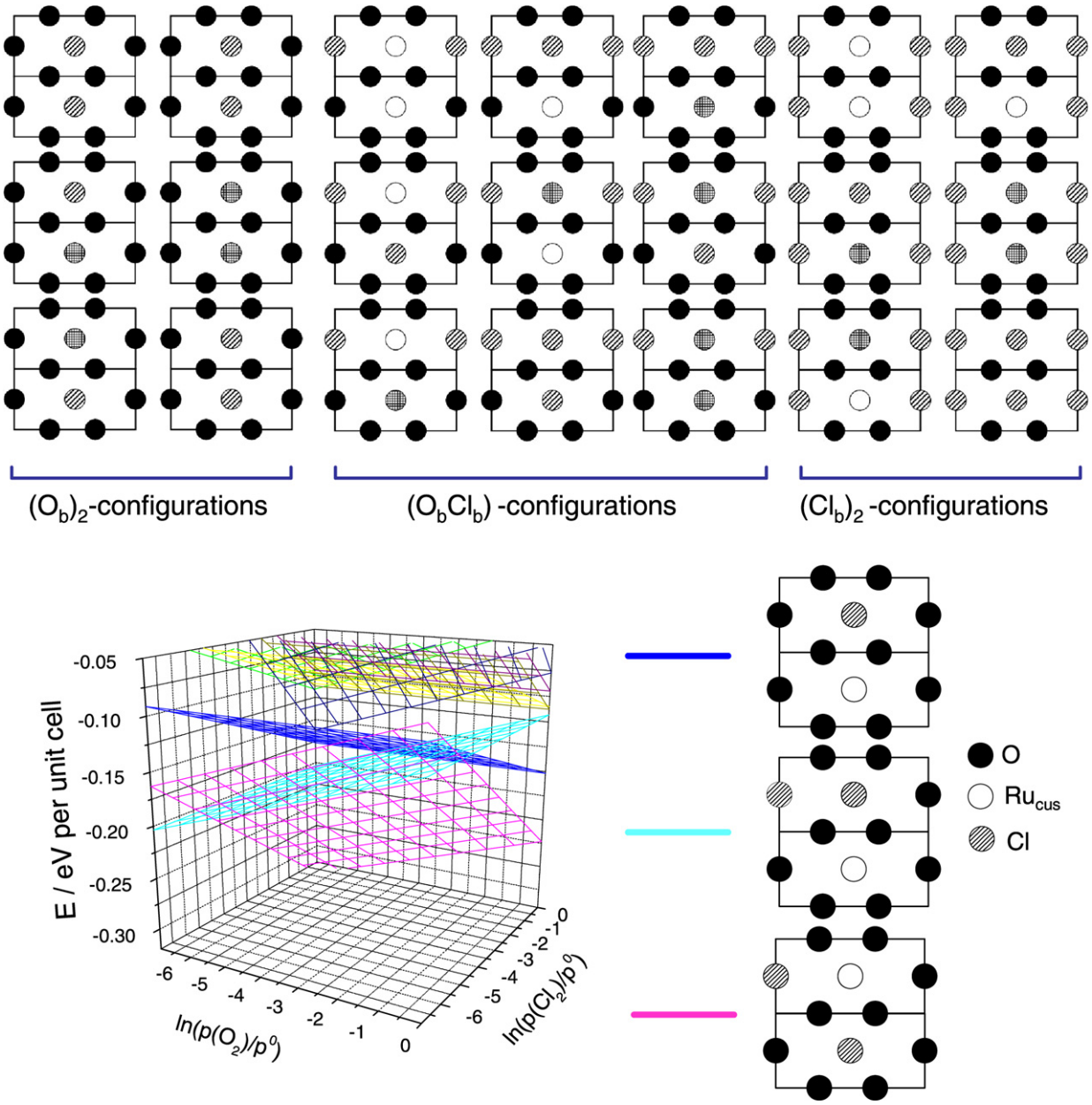

Fig. 7. Schematic models included in the *ab initio* thermodynamics diagram of the surface composition of $RuO_2(110)$ as a function of the partial O_2 and Cl_2 pressures at 573 K.

initial configuration, HCl can point towards the O_{cus} atom leading to a hydroxyl group on a Ru_{cus} site (O_{cus}–H) and a chlorine atom on a neighboring Ru_{cus} site (Cl_{cus}). The initial state is stabilized by −0.47 eV with respect to the gas-phase molecule and the relevant distances are $d(O_{cus}–H) = 1.659$, $d(H–Cl) = 1.356$, and $d(Cl–Ru_{cus}) = 2.641$ Å. The O_{cus}-assisted H abstraction is exothermic by −0.75 eV, slightly smaller than the O_b-assisted H abstraction (−0.98 eV). In the final state, the $d(O_{cus}–H) = 0.994$ and $d(Cl–Ru_{cus}) = 2.358$ Å. The transition state is 0.11 eV over reactants and the distances are $d(O_{cus}–H) = 1.684$, $d(H–Cl) = 1.351$, and $d(Ru_{cus}–Cl) = 2.640$ Å.

In summary, the barriers for hydrogen abstraction from HCl are small over both $p(2 \times 1)$-$RuO_2(110)$ and $p(2 \times 1)$-$RuO_2(110)$-O_{cus} or Cl_{cus} and thus can easily occur at any condition studied here. In good correspondence, Hisham and Benson [17] concluded that the chlorination step is fast over most single oxides.

4.3.2. Chlorine recombination

Recombination of adsorbed atomic chlorine (Eq. (4)) has been studied for several conditions (Fig. 9). First, a regular surface with a $p(2 \times 1)$ unit cell was employed with both Ru_{cus} sites covered by Cl_{cus}. However, a chlorine atom can substitute an O_b in the RuO_2 structure (Cl_b), being able to recombine with Cl_{cus} atom at a Ru_{cus} site. The recombination of two Cl_{cus} starts by the approach of one of the chlorine atoms to the sec-

ond followed by evolution of gas-phase Cl_2. The direct process is endothermic by $E^d = 1.56$ eV on the clean surface. The Cl_{cus} + Cl_b recombination is much more endothermic, 3.20 eV. Thus

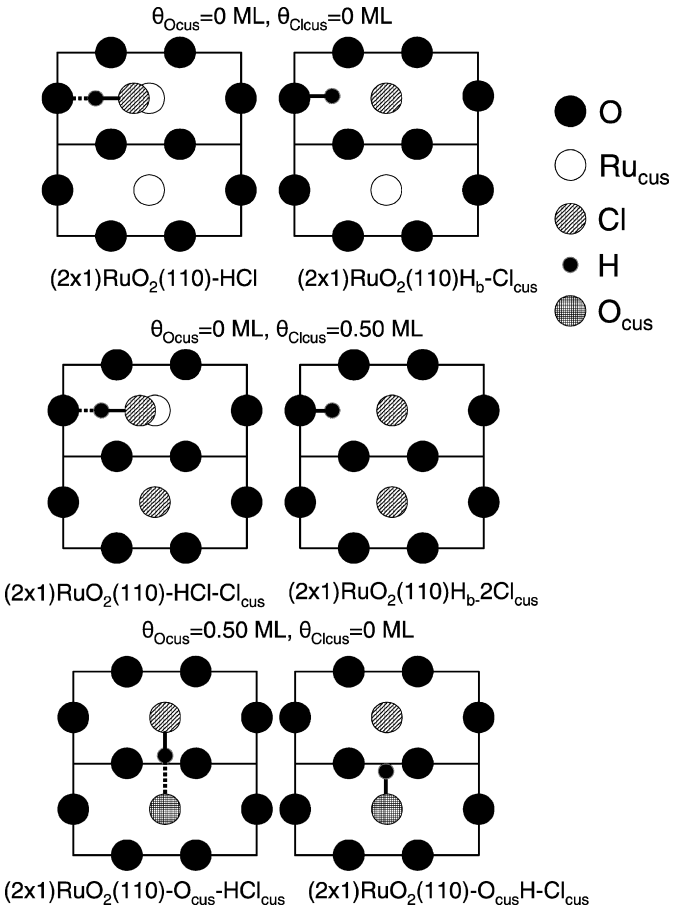

Fig. 8. Schematic representation of the initial and final states for hydrogen abstraction from HCl on $RuO_2(110)$ at two different oxygen/chlorine coverages.

the latter process is not feasible under the experimental conditions applied in the experiments.

For the Cl_{cus} + Cl_{cus} reaction, the effect of excess O_{cus} and Cl_{cus} on the neighboring Ru_{cus} sites has been studied in the $p(4 \times 1)$ supercell varying the amount of extra X_{cus} = O_{cus} and/or Cl_{cus} on the surface: $\theta_{X_{cus}} = 0$, 0.25, and 0.50 ML (Fig. 10). For the clean $RuO_2(110)$ surface, a desorption energy $E^d = 1.80$ eV was found. The presence of O_{cus} (Cl_{cus}) significantly lowered the energy required for Cl + Cl recombination, from 1.80 eV at $\theta_{O_{cus}} = 0$ to 1.26 eV at $\theta_{O_{cus}} = 0.50$ ML or 1.37 eV at final $\theta_{Cl_{cus}} = 0.50$ ML. Thus the endothermicity of the reaction can be largely affected by the quality of the surface, i.e. the degree of oxidation or chlorination. This implies a positive effect of O_{cus} and/or Cl_{cus} on Cl_2 production due to easier chlorine recombination. This fact might (at least partially) account for the increased Cl_2 production at higher O_2 pressures in Fig. 3.

Regarding technical issues, Cl_2 recombination calculated in the small $p(2 \times 1)$ supercell (open circle at $\theta_{O_{cus}} = 0$ in Fig. 10) leads a value of $E^d = 1.56$ eV. This is due to the presence of spurious lateral repulsions in this cell and indicates that one should take precautions when using small supercells to study this process. This is critical here, as chlorine recombination is the most energetically demanding step in the proposed Deacon scheme. Finally, the absolute values for adsorption/desorption energies are known to be affected by systematic errors due to inaccuracies in the functional [36]. However, the dependence of the recombination energy with the total coverage found in Fig. 10 should be seen as a derivative of the energy and is thus less affected by systematic errors. In conclusion, the trend in Fig. 10 reflects a physical situation.

4.3.3. Water formation

H_2O is formed by recombination of surface hydroxyl groups followed by desorption (Eqs. (5) and (6)). Firstly, H is trans-

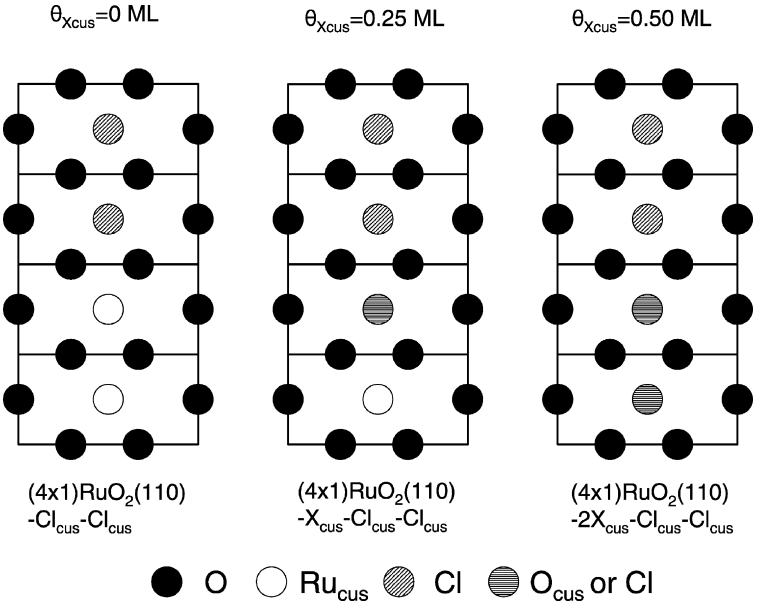

Fig. 9. Schematic representation of the initial states for atomic chlorine recombination on $RuO_2(110)$. In this case a $p(4 \times 1)$ cell is employed and three different extra O coverages.

ferred from O_bH to O_{cus}. In a second step, hydroxyl recombination was studied. These processes are visualized in Fig. 11. Since O_b atoms are difficult to remove from the $RuO_2(110)$ surface, recombination has only been studied as $O_bH + O_{cus}H$ to yield O_b and a water molecule sitting at the Ru_{cus} site followed by water desorption. The same process can also take place between two hydroxyl groups on the Ru_{cus} sites, hydroxyl recombination and water desorption was also examined for this case (*vide infra*).

Hydrogen transfer from the O_b–H to the O_{cus} site is only exothermic by −0.01 eV. At the initial state the $d(O_b–H) = 0.982$ Å, i.e. typical from a hydroxyl group. The $d(O_{cus}–H) = 2.149$ Å and the $d(O_{cus}–Ru_{cus}) = 1.752$ Å. The hydrogen transfer is hindered by a barrier of 0.55 eV (0.56 eV for the inverse barrier). At the transition state, the distances between the hydrogen and oxygen atoms are $d(O_b–H) = 1.264$ and $d(O_{cus}–H) = 1.210$ Å, respectively. The O_{cus}–Ru_{cus} bond is distorted to assist hydrogen transfer and the corresponding distance is 1.849 Å. At the final state, the $d(O_b–H)$ is enlarged to 2.453 Å and the hydroxyl group distance is $d(O_{cus}–H) = 0.978$ Å, while the bonding distance in the Ru_{cus}–$O_{cus}H$ group is 1.942 Å. If chlorine is present in the neighboring Ru_{cus} site the energy for the reaction is −0.03 eV while the barrier is 0.48 eV; thus the effect of Cl_{cus} is very small.

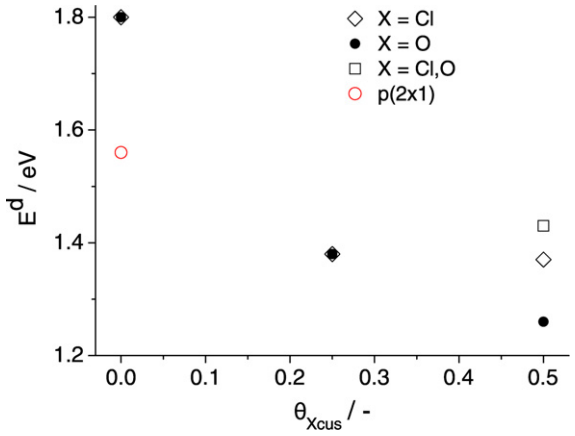

Fig. 10. Recombination energy of chlorine atoms to gas-phase Cl_2 as a function of the coverage X_{cus} = O, Cl on $RuO_2(110)$.

The second hydrogen transfer can be described as follows: $O_b–H + O_{cus}–H \rightarrow O_b + H_2O_{cus}$ (Fig. 11, bottom). The energy at the transition state is 0.38 eV higher than reactants and the overall process is slightly endothermic, 0.27 eV. In the final structure a water molecule is sitting at a Ru_{cus} site. The desorption energy of the water molecule is 0.67 eV. If a Cl_{cus} atom is present in the neighboring Ru_{cus} site the energies are slightly affected, the hydrogen transfer process is exothermic by 0.16 eV due to the formation of a Cl–H_2O interaction in the final state, and the barrier is lowered to 0.08 eV. However, this is compensated by the largest desorption energy of water, 0.90 eV. The recombination of two hydroxyl groups in neighboring Ru_{cus} sites ($O_{cus}–H + O_{cus}–H \rightarrow O_{cus} + H_2O_{cus}$) can be also considered (not shown in Fig. 11). This may correspond to the high oxygen coverage regime. At the initial state the H–O_{cus} distance is 1.878 Å while at the transition state the H atom is placed at 1.287 and 1.183 Å from both O_{cus} atoms. The transition state is only 0.24 eV higher in energy than reactants and the process is exothermic by −0.11 eV. Water desorption in this case is endothermic by 0.90 eV. The larger endothermicity found for water desorption is associated with the formation of hydrogen bonds. Our results leading to small barriers for hydroxyl recombination are in agreement with previous calculations and experimental results [24–26].

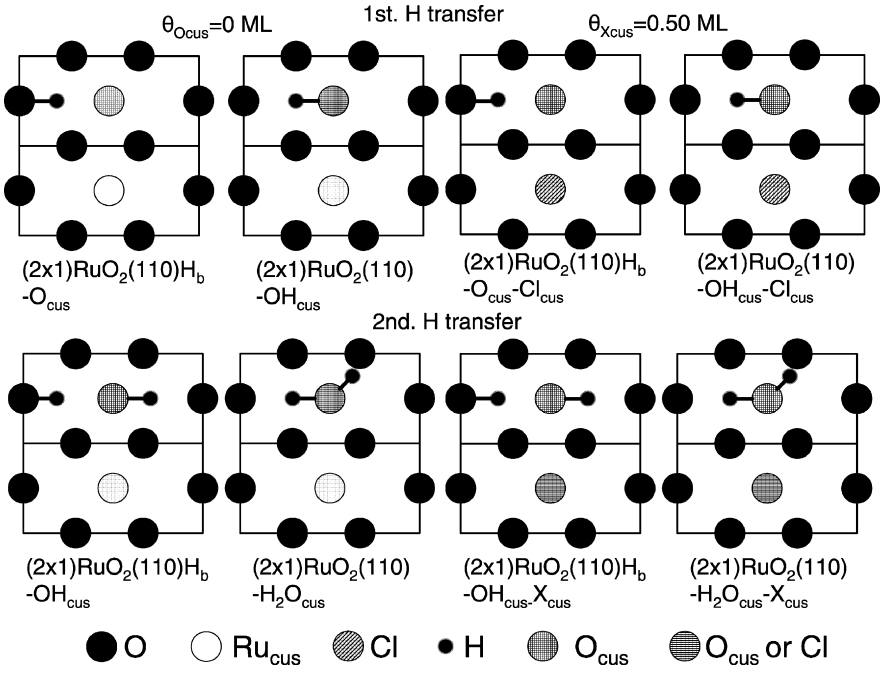

Fig. 11. Schematic representation of the initial and final states for hydrogen transfer for water formation at the Ru_{cus} site on $RuO_2(110)$. Top: $O_b–H + O_{cus} \rightarrow O_b + O_{cus}H$; and bottom $O_b–H + O_{cus}H \rightarrow O_b + H_2O_{cus}$.

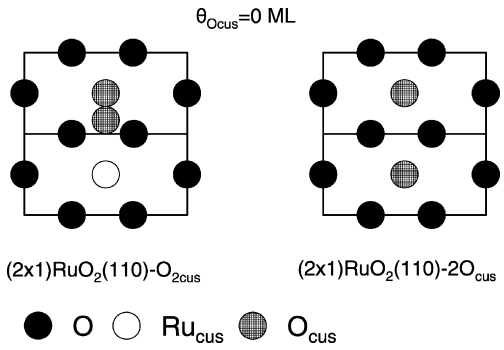

Fig. 12. Schematic representation of the initial and final states for O_2 dissociation on $RuO_2(110)$.

4.3.4. Surface reoxidation

In order to complete the catalytic cycle, the surface O_{cus} atoms on the surface need to be regenerated by dissociative adsorption of gas-phase O_2 (Eq. (7)). This is similar to what happens for CO oxidation on this surface and has been quoted as Mars–van Krevelen mechanism [19]. We have experimentally observed that the Cl_2 production fades away when no O_2 is available in the feed gas (see Fig. 3). The O_2 dissociation on the Ru_{cus} sites leading to two O_{cus} atoms has been studied. The O_2 molecule has been adsorbed on different configurations over the Ru_{cus} rows of the RuO_2 surface. The O_{2cus} tilted is adsorbed by -0.47 eV and can be considered as the precursor for dissociation (Fig. 12, left). In the O_{2cus} configuration, the O–O distance is 1.307 Å, thus close to a superoxo O_2^- species, the shortest O–Ru_{cus} distance is 2.044 and the longest 2.498 Å, from the second O to the free Ru_{cus}. The transition state structure is located 0.38 eV higher in energy than the initial state. In the structure, the O–Ru_{cus} distance is 1.891 Å while the second O–Ru_{cus} is 1.883 Å and the O–O distance is enlarged to 1.670 Å. The final structure is 0.76 eV more stable than the O_{2cus} and consists in $2O_{cus}$. The effect of surface coverage has been explored in a similar way as for Cl_2 formation, i.e. in a $p(4 \times 1)$ supercell and with various Cl_{cus} and O_{cus} coverages. The adsorption energy of the precursor state O_{2cus} molecule is reduced with respect to the clean surface, < -0.20 eV. The transition state lays about 0.4 eV higher in energy than the precursor state, while the final state is about -0.65 eV lower in energy than the reactants. The surface coverage effect on O_2 dissociation is to reduce the binding energy of the precursor to the surface.

Finally, in the reaction network, O_2 readsorption is the only step requiring two empty Ru_{cus} sites. As we have seen in the computational characterization of the surface (Section 3), two neighboring empty Ru_{cus} sites might not be abundant at high Cl_2 and O_2 pressures. Consequently, surface oxidation may become a difficult step in the reaction. This latter aspect might be partially responsible for the dependence observed between the Cl_2 production over RuO_2 and the partial O_2 pressure in the feed mixture (Fig. 3).

The nature of the active oxygen on the $RuO_2(110)$ surface has been a matter of extensive discussion [23,55]. Our calculations point out to the dual role of the oxygen on the surface. The lattice oxygen O_b can act as a proton scavenger for the HCl molecule and as a hydroxyl reservoir in water formation. However, structural oxygen in ruthenium oxide (O_b) cannot be removed as water (H_2O_b) and therefore cannot oxidize by itself hydrogen chloride. In contrast, O_{cus} can act as proton scavenger, forming hydroxyl groups on the surface and water molecules. The binding energy of the latter is low enough so they can desorb under reaction conditions.

5. Conclusions

DFT calculations in combination with experiments have been used to study the HCl oxidation to Cl_2 (Deacon process) over RuO_2. Activity tests in a fixed-bed reactor at ambient pressure demonstrated that RuO_2 powder is a highly active catalyst for Cl_2 production. Characterization of the fresh and used RuO_2 revealed no appreciable alteration of the bulk structure and limited chlorination of the sample, in agreement with *ab initio* thermodynamics. The Deacon reaction has been described by a Mars–van Krevelen type reaction mechanism consisting of five elementary steps: hydrogen abstraction from HCl, recombination and desorption of atomic chlorine, hydroxyl recombination, water desorption, and oxygen adsorption. Atomic chlorine recombination to yield gas-phase Cl_2 is the most energy-demanding step. In addition, surface reoxidation can be blocked by high surface coverages. Reaction conditions (mainly partial pressures and temperature) will determine whether the rate-determining step of the Deacon process is chlorine recombination or oxygen readsorption. Further clarification of this aspect requires more specific mechanistic and kinetic studies. Finally, we have experimentally observed a larger Cl_2 production upon increasing the feed O_2:HCl ratio. Based on our calculations, this trend is tentatively attributed to both the increase of O coverage on the surface at higher partial O_2 pressures and the reduced energy for chlorine formation at high coverages.

Acknowledgments

Financial support from the Spanish MEC (projects CTQ-2006-01562/PPQ, CTQ2006-00464BQU, and Consolider-Ingenio 2010, grant CSD2006-003) and the Generalitat de Catalunya is acknowledged. The authors thank BSC and RES-CesViMa for computing time.

References

[1] S. Motupally, D.T. Mah, F.J. Freire, J.W. Weidner, Electrochem. Soc. Interface 7 (3) (1998) 32.
[2] H. Deacon, U.S. Patent 165,802, 1875.
[3] H.F. Johnstone, Chem. Eng. Prog. 44 (1948) 657.
[4] H.Y. Pan, R.G. Minet, S.W. Benson, T.T. Tsotsis, Ind. Eng. Chem. Res. 33 (1994) 2996, and references therein.
[5] A.J. Johnson, A.J. Cherniavsky, U.S. Patent 2,542,961, 1951.
[6] F. Wattimena, W.M.H. Sachtler, Stud. Surf. Sci. Catal. 7 (1981) 816.
[7] T. Yasuaki, Stud. Surf. Sci. Catal. 92 (1995) 41.
[8] H. Itoh, Y. Kono, M. Ajioka, S. Takezaka, M. Katzita, U.S. Patent 4,803,065, 1989.
[9] T. Kiyoura, Y. Kogure, T. Nagayama, K. Kanaya, U.S. Patent 4,822,589, 1989.

[10] R.G. Minet, S.W. Benson, M.K. Mortensen, T.T. Tsotsis, WO 97/11026.
[11] M. Mortensen, R.G. Minet, T.T. Tsotsis, S.W. Benson, Chem. Eng. Sci. 54 (1999) 2131.
[12] U. Nieken, O. Watzenberger, Chem. Eng. Sci. 54 (1999) 2619.
[13] T. Hibi, T. Okuhara, K. Seki, H. Abekawa, H. Hamamatsu, WO 01/10550, 2001.
[14] T. Arikawa, Y. Murakami, Y. Takasu, J. Appl. Electrochem. 28 (1998) 511.
[15] V.V. Panic, A. Dekanski, S.K. Milonjic, R.T. Atanasoski, B.Z. Nikolic, Colloids Surf. A 157 (1999) 269.
[16] K. Iwanaga, K. Seki, T. Hibi, K. Issoh, T. Suzuta, M. Nakada, Y. Mori, T. Abe, Sumitomo Kagaku (2004) 4.
[17] M.W.M. Hisham, S.W. Benson, J. Phys. Chem. 99 (1995) 6194.
[18] A.G. Aglulin, Kinet. Catal. 39 (1998) 521.
[19] H. Over, Y.D. Kim, A.P. Seitsonen, S. Wendt, E. Lundgren, M. Schmid, P. Varga, A. Morgante, G. Ertl, Science 287 (2000) 1474.
[20] L. Wang, H. Kisch, Angew. Chem. Int. Ed. 39 (2000) 3921.
[21] H. Madhavaram, H. Idriss, S. Wendt, Y.D. Kim, M. Knapp, H. Over, J. Aßmann, E. Löffler, M. Muhler, J. Catal. 202 (2001) 296.
[22] J. Assmann, E. Löffler, A. Birkner, M. Mühler, Catal. Today 85 (2003) 235.
[23] K. Reuter, M. Scheffler, Phys. Rev. B 73 (2006) 045433.
[24] J.H. Wang, C.Y. Fan, Q. Sun, K. Reuter, K. Jacobi, M. Scheffler, G. Ertl, Angew. Chem. Int. Ed. 42 (2003) 2151.
[25] M. Knapp, D. Crihan, A.P. Seitsonen, E. Lundgren, A. Resta, J.N. Andersen, H. Over, J. Phys. Chem. C 111 (2007) 5363.
[26] M. Knapp, D. Crihan, A.P. Seitsonen, H. Over, J. Am. Chem. Soc. 127 (2005) 3236.
[27] Y. Wang, K. Jacobi, W.-D. Schoene, G. Ertl, J. Phys. Chem. B 109 (2005) 7883.
[28] I. Balint, A. Miyazaki, K.-I. Aika, J. Catal. 220 (2003) 74.
[29] B.-Z. Zhan, M.A. White, T.-S. Sham, J.A. Pincock, R.J. Doucet, K.V.R. Rao, K.N. Robertson, T.S. Cameron, J. Am. Chem. Soc. 125 (2003) 2195.
[30] H. Liu, E. Iglesia, J. Phys. Chem. B 109 (2005) 2155.
[31] S. Yang, Y. Feng, J. Wan, W. Zhu, Z. Jiang, Appl. Surf. Sci. 246 (2005) 222.
[32] K. Villani, C.E.A. Kirschhock, D. Liang, G. Van Tendeloo, J.A. Martens, Angew. Chem. Int. Ed. 45 (2006) 3106.
[33] S. Brunauer, P.H. Emmet, E. Teller, J. Am. Chem. Soc. 60 (1938) 309.
[34] G. Kresse, J. Hafner, Phys. Rev. B 47 (1993) 558.
[35] G. Kresse, J. Furthmüller, Phys. Rev. B 54 (1996) 11169.
[36] B. Hammer, L.B. Hansen, J.K. Nørskov, Phys. Rev. B 59 (1999) 7413.
[37] G. Kresse, D. Joubert, Phys. Rev. B 59 (1999) 1758.
[38] R.W.G. Wyckoff, Crystal Structures, vol. 1, second ed., Wiley, New York, 1963.
[39] C.E. Boman, Acta Chem. Scand. 24 (1970) 116.
[40] A. Kiejna, G. Kresse, J. Rogal, A. De Sarkar, K. Reuter, M. Scheffler, Phys. Rev. B 73 (2006) 035404.
[41] Y.D. Kim, S. Schwegmann, A.P. Seitsonen, H. Over, J. Phys. Chem. B 105 (2001) 2205.
[42] H.J. Monkhorst, J.D. Pack, Phys. Rev. B 13 (1976) 5188.
[43] G. Henkelman, B.P. Uberuaga, H. Jónsson, J. Chem. Phys. 113 (2000) 9901.
[44] K. Reuter, M. Scheffler, Phys. Rev. B 68 (2003) 045407.
[45] X.G. Wang, A. Chaka, M. Scheffler, Phys. Rev. Lett. 84 (2000) 3650.
[46] Z. Łodziana, J.K. Nørskov, P. Stoltze, J. Chem. Phys. 118 (2003) 11179.
[47] NIST webpage http://webbook.nist.gov/chemistry, September 2007.
[48] G.E. Gibson, N.S. Bayliss, Phys. Rev. 44 (1933) 188.
[49] S. Hubinger, J.B. Nee, J. Photochem. Photobiol. A 86 (1995) 1.
[50] J.B. Burkholder, E.J. Bair, J. Phys. Chem. 87 (1983) 1859.
[51] G. Wulff, Z. Krystallogr. Miner. 34 (1901) 449.
[52] M. Ramamoorthy, D. Vanderbilt, R.D. King-Smith, Phys. Rev. B 46 (1994) 16721.
[53] H. Over, M. Gierer, H. Bludau, G. Ertl, S.Y. Tong, Surf. Sci. 314 (1994) 243.
[54] P. van der Avert, S.G. Podkolzin, O. Manoilova, H. de Winne, B.M. Weckhuysen, Chem. Eur. J. 10 (2004) 1637.
[55] S. Wendt, M. Knapp, H. Over, J. Am. Chem. Soc. 126 (2004) 1537.